On the effectiveness of elastic wave measurements for monitoring the response of caprocks

On the effectiveness of elastic wave measurements for monitoring the response of caprocks

by

Andrea Ciancimino[1*], Sebastiano Foti[2], Giorgio Volontè[3], Guido Musso[4]

[1*]Corresponding author, Politecnico di Torino, Turin, Italy; andrea.ciancimino@polito.it; 0000-0001-8955-4605

[2]Politecnico di Torino, Turin, Italy; sebastiano.foti@polito.it; 0000-0003-4505-5091

[3]Eni SpA, Milan, Italy; giorgio.volonte@eni.com; 0000-0002-6942-7198

[4]Politecnico di Torino, Turin, Italy; guido.musso@polito.it; 0000-0003-3151-4058

Abstract

This study investigates the effectiveness of elastic wave measurements in tracking the mechanical degradation of a structured clay under monotonic and cyclic loading. Triaxial tests were carried out on both intact and reconstituted specimens monitoring the evolution of the material state through ultrasonic transducers. The S-wave propagation velocity V_S is shown to be affected by limited variations (< 6%). This can be explained considering that material destructuration occurs in a rather narrow shear band. Conversely, the normalized cross-correlation coefficient $\hat{\rho}_S$ appears to be a more sensitive indicator of structural degradation, showing a significant decrease – up to 40% – as failure is approaching. Such an effect reflects the changes in signal amplitude and shape associated with the formation of the shear band. The $\hat{\rho}_S$ evolution also mimics brittle and ductile responses, demonstrating its potential as a robust parameter for monitoring the in-situ state of caprocks in underground storage applications.

Keywords

Underground gas storage; wave measurements; monitoring; fabric/structure of soils; cyclic triaxial tests; UN SDG 7: AFFORDABLE AND CLEAN ENERGY; UN SDG 13: CLIMATE ACTION

1 Introduction

Innovative geomechanics applications include exploiting depleted hydrocarbon reservoirs to store natural gas or hydrogen for use as an energy vector (e.g., Aminu et al., 2017; Heinemann et al., 2021). Such applications pose several challenges due to complex interactions between reservoir and non-native fluids. For example, seasonal storage operations can induce cyclic loadings on the caprock, potentially compromising its sealing integrity (e.g. Jeanne et al., 2020). Reliable monitoring systems are therefore essential to assess the impact of such operations.

Elastic wave properties are promising monitoring parameters, as the small-strain stiffness of geomaterials is strongly influenced by their state in terms of void ratio, saturation degree, stress state and structure, the latter intended as a combination of particle arrangement and interparticle bonding (e.g., Santamarina et al., 2001; Clayton, 2011). Upon chemo-hydro-mechanical loading, the material state evolves, leading to changes in elastic stiffnesses and hence in wave propagation parameters (e.g., Shibuya, 2000; Falcon-Suarez et al., 2016). This has been widely observed in laboratory studies on soils and rocks under monotonic (e.g., Stanchits et al., 2006; Montoya & De Jong, 2015; Dutta et al., 2020) and cyclic (e.g., Zhou & Chen, 2005; Xiao et al., 2010) loadings.

Wave velocity measurements are also attractive as wellbore sonic logs are typically recorded for site characterization during hydrocarbon production operations. However, a potential limitation lies in the small changes often observed in structured soils and rocks as failure approaches (e.g. Stanchits et al., 2006; Montoya & De Jong, 2015). This paper proposes an alternative approach based on changes in shape and amplitude of the recorded signals. The methodology is applied to wave measurements taken alongside monotonic triaxial testing on either intact or reconstituted caprock specimens to highlight the differences between brittle or more ductile responses. To demonstrate its effectiveness in relation to fatigue loading, the technique is then applied to cyclic triaxial tests.

2 Materials and methods

Monotonic and cyclic consolidated undrained triaxial tests were performed on Santerno clay, a clayey caprock from the Po valley in Italy (e.g. Benetatos et al., 2023), retrieved from a depth of approximately 1150 m and characterised by a relevant post-sedimentation structure.

The tests were carried out using the medium pressure triaxial apparatus of the Politecnico di Torino (see Barla et al., 2010). The testing protocol included an initial saturation stage which involved a flushing step and a back-pressure sequence. This ensured that the specimen and the drainage lines were completely saturated. The back-pressure procedure was considered concluded when Skempton's B-values larger than 0.97 were achieved. Thereafter, the specimens were subjected to anisotropic consolidation. Intact specimens were consolidated up to the expected lithostatic stresses: $p'_0 = 8.1$ MPa and $q_0 = 6.3$ MPa, except one which was consolidated at twice the in-situ stress. The lithostatic stress state at the relevant depth was computed by integrating direct borehole measurements with the analysis of log data (Ciancimino et al., 2024). Reconstituted specimens were prepared by starting from a slurry composed of the same material with a water content of 1.5 times the liquid limit, compacted one-dimensionally to an axial effective stress $\sigma'_{ax} = 9$ MPa, and then triaxially consolidated to p'_0 and q_0. The consolidation of test MR-TX 01 included a loading-unloading step at constant stress ratio q_0 / p'_0 to achieve an over-consolidation ratio $OCR = 1.5$. Monotonic compression tests were performed by imposing constant axial strain rates $\dot{\varepsilon}_{ax}$ of either 0.01 %/min or 0.0005 %/min, while cyclic stress-controlled tests imposed one-way sinusoidal deviatoric loadings of amplitude A, with a maximum deviator q_{max}, a mean deviator $q_{mean} = q_{max} - A$, and a period $T = 5$ min (corresponding to a frequency of 0.0033 Hz).

A summary of the tests is given in Table 1. More details about the experimental procedures and setup, along with a comprehensive analysis of the time-dependent monotonic and cyclic response of the material can be found in Ciancimino et al. (2024; 2026).

Table 1: Summary of the anisotropically consolidated undrained triaxial tests

ID	*Material*	$\dot{\varepsilon}_{ax}$: %/min	p'_0 : MPa	q_0 : MPa	q_{max} : MPa	A : MPa	N_f	*Reference*
MI-TX 01	Intact	0.0005	8.1	6.3	-	-	-	Ciancimino et al. (2024)
MI-TX 02	Intact	0.01	16.2	12.6	-	-	-	This study
MR-TX 01	Reconstituted $OCR = 1.5$	0.0005	8.1 (12.2)†	6.3 (9.5)†	-	-	-	This study
MR-TX 02	Reconstituted NC	0.01	8.1	6.3	-	-	-	This study
CI-TX 01	Intact	-	8.1	6.3	13	3.25	18	Ciancimino et al. (2024)
CI-TX 09	Intact	-	8.1	6.3	12.5	4.25	173	Ciancimino et al. (2026)

† Maximum stress applied during the consolidation stage

The top cap and the base of the device are instrumented with compression (P-wave) and shear (S-wave) transducers, which can receive and transmit high-frequency ultrasonic pulses. The measurements were carried out by imposing as input signal a square pulse with a 1 μs duration. Signals were recorded with a scan time of 500 μs and a sample time of $8 \cdot 10^{-3}$ μs.

For both P- and S-waves, the received signals were processed based on a reference scan x_0 recorded at the end of consolidation. For this scan, the first-arrival time t_0 is obtained by manually picking out signals with reverse polarization, in order to identify the instant at which the recorded waves appear coherent with each other. To illustrate this, Figure 1 shows the manual picking carried out for P- and S-wave reference signals for test MI-TX 01. It should be noted that the exact definition of t_0 has only a minor impact on the results, as the analysis focuses more on relative variations in wave parameters than absolute values.

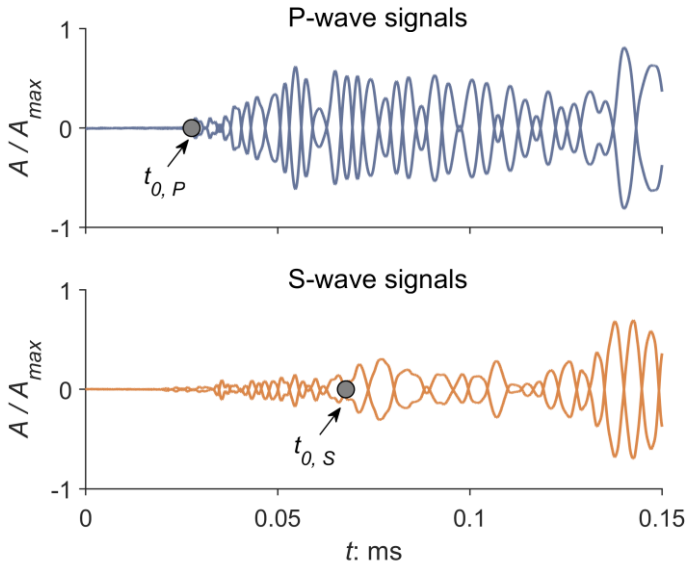

Figure 1: P- and S-wave reference signals with reverse polarization taken during test MI-TX 01

For any other scan x_i, the variation of the first-arrival time Δt_i is obtained by a cross-correlation algorithm. Specifically, x_i is shifted by a tentative time-lag m, and the normalized cross-correlation coefficient $\rho(x_0, x_i)$ is calculated:

$$\rho(x_0, x_i) = \frac{R_{x_0,x_i}(m)}{\sqrt{R_{x_0,x_0}(0) \cdot R_{x_i,x_i}(0)}} \tag{1}$$

where $R_{x_0,xi}(m)$ denotes the cross-correlation of signals x_0 and x_i, with x_i shifted by m. The time-lag Δt_i is identified as the m value associated with the maximum normalized coefficient $\hat{\rho}(x_0, x_i)$. When analysing two

identical signals shifted in time, $\hat{\rho}(x_0, x_i) = 1$. In general, x_0 and x_i differ in shape and amplitude, with $\hat{\rho}(x_0, x_i)$ somehow reflecting these variations.

The first-arrival time t_i for the x_i signal and the associated propagation velocity are therefore:

$$t_i = t_0 + \Delta t_i \tag{2}$$

$$V_i = \frac{H_i}{t_i} \tag{3}$$

with H_i being the current specimen height measured using an external transducer calibrated to eliminate spurious displacements caused by the deformability of the apparatus (after Ciancimino et al., 2026).

The above procedure applies to signals acquired for both P- and S-waves, resulting in the corresponding coefficients $\hat{\rho}_P$ and $\hat{\rho}_S$, and velocities V_P and V_S. Figure 2 shows its application for two pairs of normalized signals acquired during test MI-TX 01. The signals at $\varepsilon_{ax} = 0$ (i.e. grey lines) were used to pick the reference times, $t_{0,P}$ and $t_{0,S}$, as shown in the upper plots along with scans taken after monotonic shearing (i.e. for ε_{ax} = 0.05). The cross-correlation was applied in a time interval ranging from 0.9 to 1.9 of the reference times to achieve a balance between robustness (since it includes a few periods) and accuracy (as non-direct waves are less likely to be observed). The bottom plots show the good match after shifting the $\varepsilon_{ax} = 0.05$ signals by the identified Δt_i values.

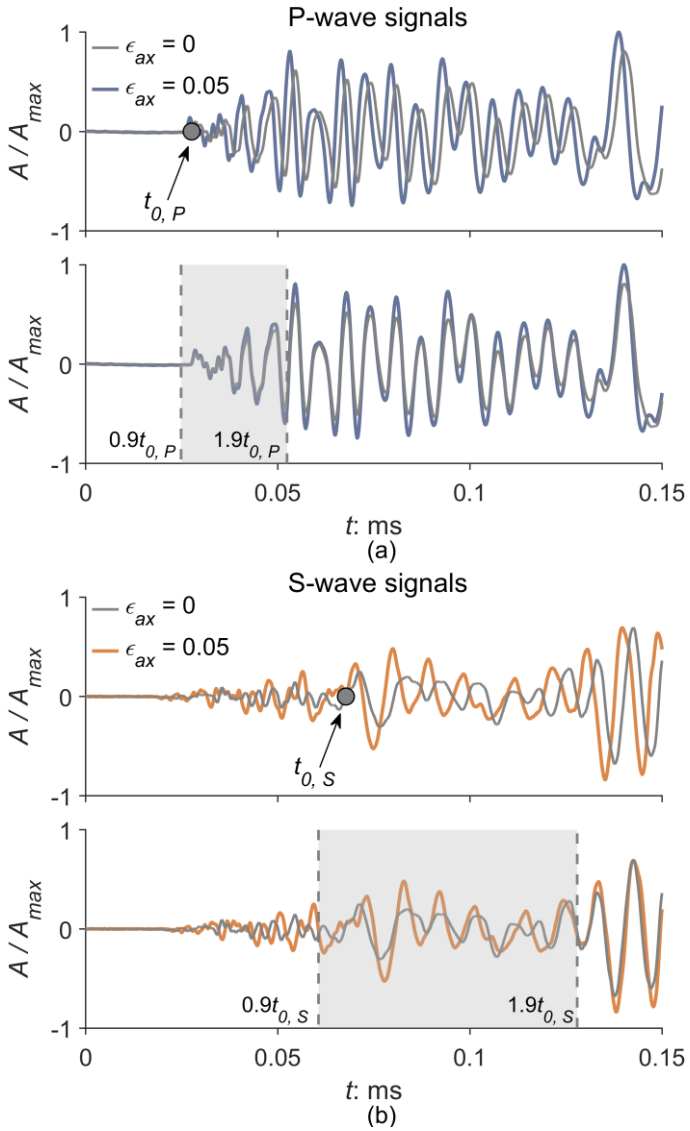

Figure 2: P- and S-wave signals (a and b plots, respectively) taken during test MI-TX 01 before the start and at the end (i.e. for $\varepsilon_{ax} = 0.05$) of the shearing phase; the upper plots show the raw data, the lower plots show the signals after realignment

Experimental studies have shown the potential impact of the selected input frequency on ultrasonic wave testing (e.g., Ferreira et al., 2021). However, preliminary checks were performed in this study, showing that results were not significantly affected by the duration of the input pulse. Indeed, the proposed technique is based on differential output signal analysis and therefore the impact of spurious wave groups is limited. Moreover, the imposed input generates a broad frequency range. For instance, the frequency spectra of the signals presented in Figure 2 are characterised by a peak amplitude at around 150 kHz for S-waves, while the peak occurs at around 120 kHz for P-waves.

It is worth mentioning that the experimental tests considered in this study were deliberately chosen to cover a wide range of material states and loading conditions (see Table 1). The relevant differences in loading protocols (e.g. monotonic or cyclic), imposed strain rate (or frequency) and initial material state (e.g. intact vs.

reconstituted) are known to result in markedly different stress-strain responses. Consequently, the selected tests provide a robust benchmark against which the capabilities and limitations of the proposed methodology can be assessed.

3 Results

3.1 Consolidation

Figure 3 shows a detailed analysis of the results of the consolidation stage for test MI TX-01. The stage lasted five days: 48 hours of primary consolidation up to p'_0 and q_0, followed by 70 hours of constant external load. ε_{ax} increases significantly up to the end of primary consolidation, after which a smoother increase is observed due to dissipation of residual excess pore pressure and creep phenomena (Figure 3a). As expected, ε_{ax} progressively stabilizes over time.

Wave measurements were taken every hour, and the data were processed adopting the last acquisition as reference. Figure 3b shows the evolution of P- and S-wave velocities normalised to the values measured at the end of consolidation, $V_{P,0}$ and $V_{S,0}$ respectively. The results mimic the ε_{ax} trends, revealing a steep increase during primary consolidation, followed by progressive stabilisation and almost constant values for the final 10 hours (shadowed zone in Figure 3).This interval was therefore used to assess the robustness and the reliability of the proposed methodology, computing the average values and the corresponding coefficients of variation which are reported in Figure 3b. The corresponding uncertainty is less than 0.1% upon stable conditions. Figure 3c shows the corresponding trends for the coefficients $\hat{\rho}_P$ and $\hat{\rho}_S$. P-wave measurements appear to be more stable, with $\hat{\rho}_P$ values just below unity. In contrast, $\hat{\rho}_S$ appears to be more affected by p', probably because of the weaker coupling between the transducers and the specimens at low pressures and the more substantial observed changes in V_S. Once again, over the last 10 hours, both values have remained almost identical, demonstrating the excellent repeatability of the wave measurements.

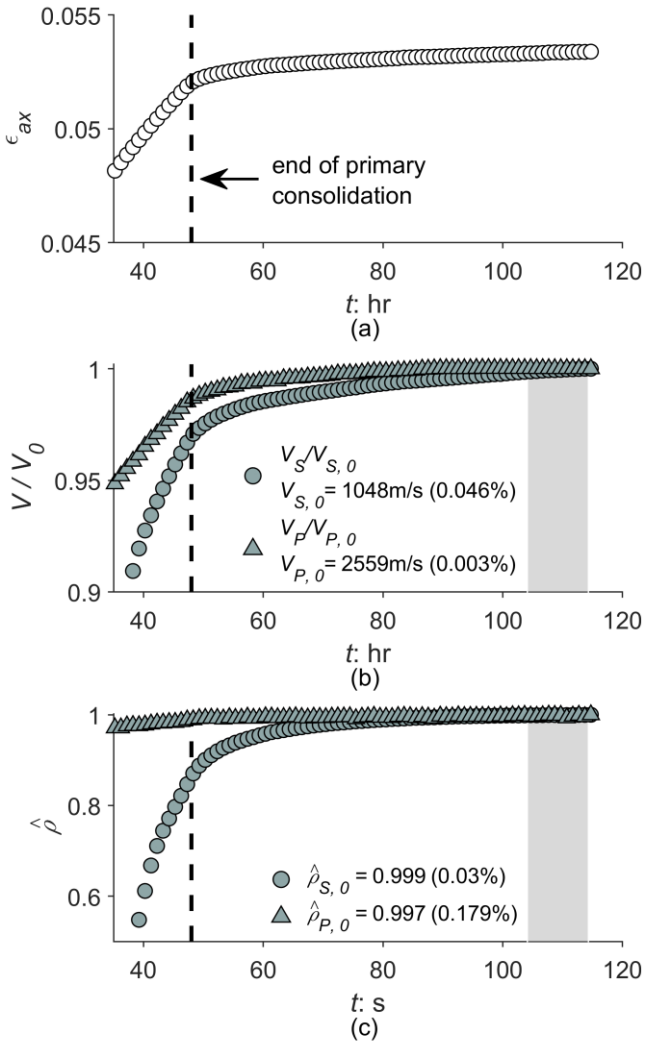

Figure 3: Evolution of the material state with time upon consolidation for test MI-TX 01 (intact material; p'_0, q_0): (a) effective mean stress p'; (b) axial strain ε_{ax}; (c) normalized P- and S-wave velocities $V_P / V_{P,0}$ and $V_S / V_{S,0}$; and (c) normalized P- and S-wave cross-correlation coefficients $\hat{\rho}_P$ and $\hat{\rho}_S$; the shaded area shows the results used to compute the average values and the associated coefficients of variation (in brackets)

Figure 4 shows, for each specimen, the evolution of the material state with σ'_{ax} in terms of void ratio e, V_P, V_S, and undrained Poisson's ratio ν_u, the latter computed as a function of V_P / V_S. V_S data are shown only over a certain range of σ'_{ax}, as S-waves were overlapped by undesired parasite waves at low pressures.

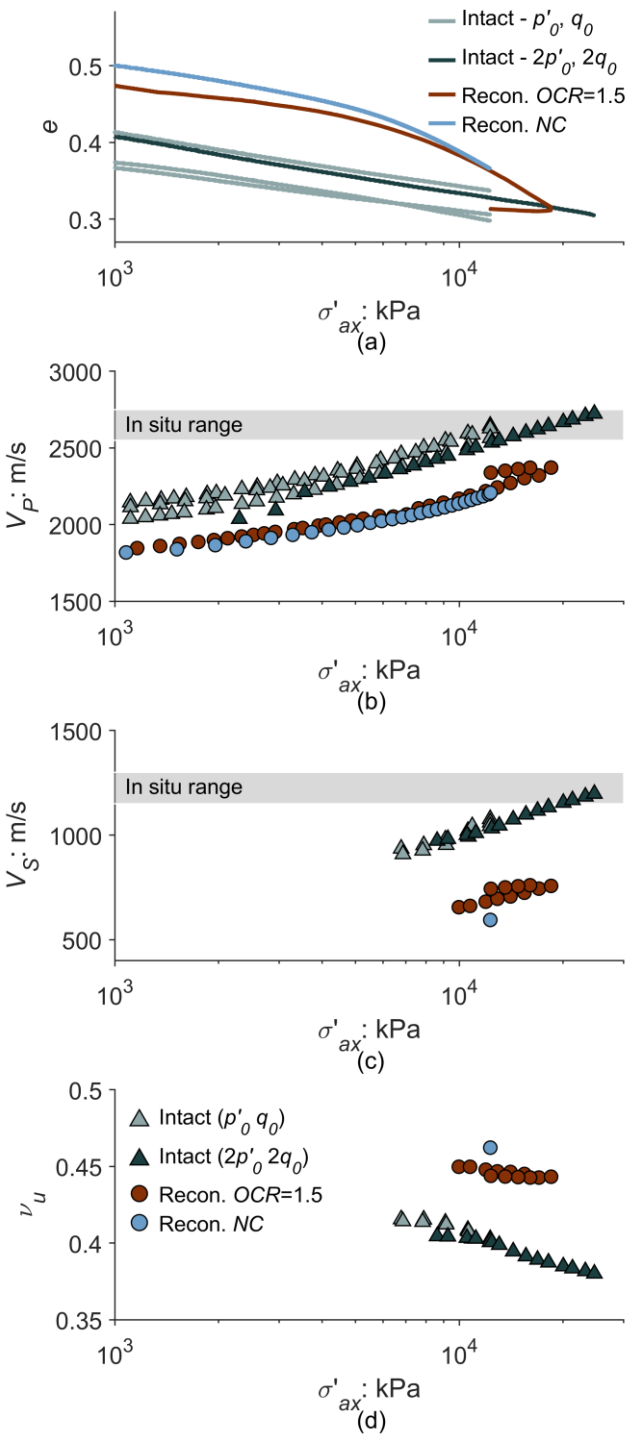

Figure 4: Evolution of the material state with σ'_{ax} upon consolidation: (a) void ratio e; (b) P-wave velocity V_P; (c) S-wave velocity V_S; and (d) undrained Poisson's ratio ν_u

Intact specimens exhibit a stiff response, suggesting that no substantial yielding occurred during the consolidation, even up to twice the in-situ state (Figure 4a). Conversely, reconstituted specimens show an elasto-plastic response for $\sigma'_{ax} > 9$ MPa, with the specimen characterized by $OCR = 1.5$ reaching a void ratio consistent with the intact material.

For intact specimens as e decreases, both V_P and V_S increase (Figure 4b-c), approaching the in-situ ranges. The latter were obtained through continuous sonic logging within the caprock formation (data after Ciancimino et al., 2024). For reconstituted specimens, a larger increase in V_P is observed after yielding. However, it never reaches the values measured for the intact material. Consolidation also induces a decrease of ν_u (Figure 4d), which is more significant for intact specimens, while it is barely visible for reconstituted ones. By the end of the consolidation, ν_u is about 0.38 and 0.45 for intact and reconstituted specimens, respectively. These differences are again attributed to the natural post-sedimentation structure, which implies a larger bulk modulus of the soil skeleton and, therefore, a lower ν_u for the intact Santerno clay. These trends are consistent with those observed in other experimental studies involving stiff clayey materials retrieved from similar or shallower depths (see, e.g., Mavko et al., 1998; Musso et al., 2015; Shibuya, 2000).

3.2 Monotonic Shear

Figure 5 presents the monotonic undrained responses in terms of q / p' against the imposed ε_{ax} upon shearing. Test MI TX-01 shows a fragile response of the intact material when consolidated at in-situ stresses. After reaching the peak shear strength, pronounced softening towards the post-rupture strength occurs due to the degradation of the natural structure and the formation of a narrow shear band (Ciancimino et al., 2024). Such brittle behaviour is partially inhibited by increasing the consolidation pressure, as shown in test MI TX-02. Conversely, whether normally consolidated (test MR TX-02) or lightly over-consolidated (test MR TX-01), the reconstituted material shows ductile behaviour. Consistently with previous findings (e.g. Burland et al., 1996), both natural and reconstituted specimens tend toward similar $q / p' = 1$ at large strains.

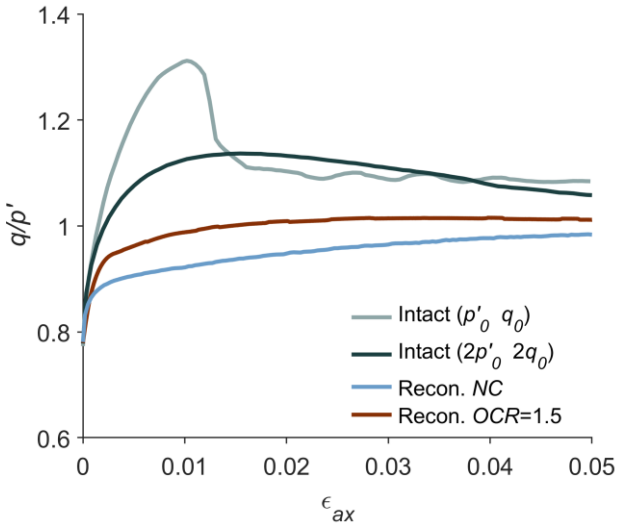

Figure 5: Results of the monotonic undrained triaxial tests on intact and reconstituted specimens of Santerno clay

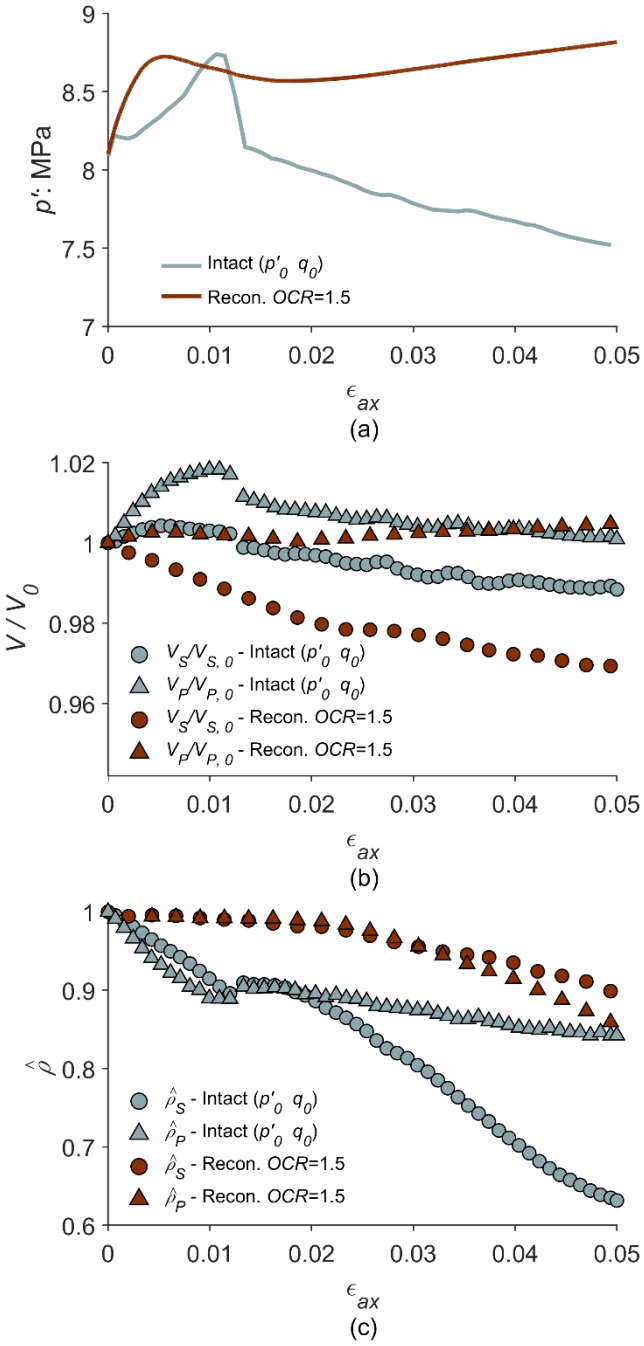

Figure 6: Evolution of the material state with imposed ε_{ax} upon monotonic shearing for tests MI-TX 01 (intact material; p'_0, q_0) and MR-TX 01 (reconstituted, $OCR = 1.5$): (a) effective mean stress p'; (b) normalized P- and S-wave velocities $V_P / V_{P,0}$ and $V_S / V_{S,0}$; and (c) normalized P- and S-wave cross-correlation coefficients $\hat{\rho}_P$ and $\hat{\rho}_S$

The material state evolution was tracked via the cross-correlation procedure. Figure 6 shows the results for tests MI-TX 01 (intact) and MR-TX 01 (reconstituted, $OCR = 1.5$), consolidated to the in-situ stress state. The propagation velocities are shown after normalization with respect to the initial values $V_{P,0}$ and $V_{S,0}$. The intact material shows an initial increase in $V_P / V_{P,0}$ and $V_S / V_{S,0}$ (Figure 6b) which is due to a corresponding increase in p' (Figure 6a). For axial strains larger than 0.015, the sudden mechanical softening produces a relatively steep decrease in the velocities, followed by a more gradual reduction. On the contrary, the

reconstituted material shows a continuous slight increase in $V_P / V_{P,0}$, probably due to the observed increase in p', while a gradual reduction in $V_S / V_{S,0}$ is observed. The distinction observed for intact and reconstituted material between a sharp or more gradual reduction in velocity closely matches with the deviatoric responses shown in Figure 5. However, the variations in propagation velocities appear to be quite small in amplitude, with a maximum decrease of about 2%.

The changes in the material state can also be inferred by means of the cross-correlation coefficients $\hat{\rho}_P$ and $\hat{\rho}_S$ (Figure 6c). For the reconstituted material, $\hat{\rho}_S$ slightly decreases. Conversely, an abrupt drop to 0.6 is observed for the intact specimen, especially after the peak shear strength is reached, reflecting the softening associated with the formation of the shear band. Similar trends can be observed for $\hat{\rho}_P$, although the drop for intact material after peak strength is attained appears much less pronounced. This difference can be attributed to the minor influence that the destructuration process has on P-waves propagating through the shear band compared to S-waves propagation. Consequently, in the following the discussion will be limited to the evolution of $\hat{\rho}_S$, even though similar but less evident patterns can be observed for $\hat{\rho}_P$. Figure 7 compares $\hat{\rho}_S$ values of test MI TX-01, with the trends obtained in tests MI TX-02 and MR TX-01, performed respectively on intact material consolidated to twice the in-situ stress state and on reconstituted normally consolidated material. Interestingly, both tests present a rather gradual reduction in $\hat{\rho}_S$. In particular, the results of test MI TX-02 suggest that $\hat{\rho}_S$ is not only a reliable indicator of progressive destructuration, as shown by the significant reduction observed, but its evolution also appears influenced by the mechanical behaviour of the material. Indeed, for test MI TX-01 it reflects the brittle nature of the mechanical response shown in Figure 5, which is somewhat inhibited by the higher consolidation pressures achieved in test MI TX-02.

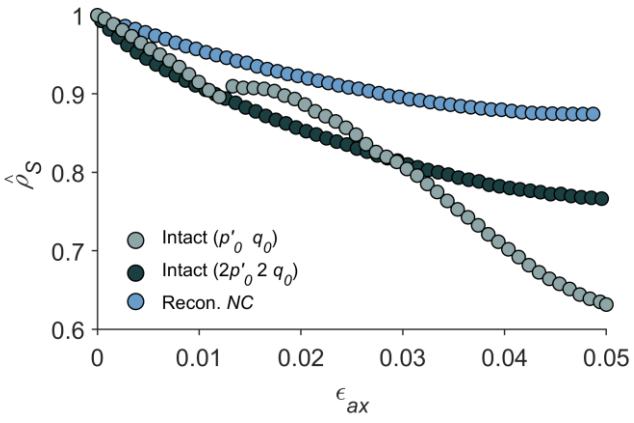

Figure 7: Evolution of the normalized S-wave cross-correlation coefficient $\hat{\rho}_S$ with imposed ε_{ax} upon monotonic shearing for tests MI-TX 01 (intact; p'_0, q_0), MI-TX 02 (intact; $2p'_0$, $2q_0$), and MR-TX 02 (reconstituted, *NC*)

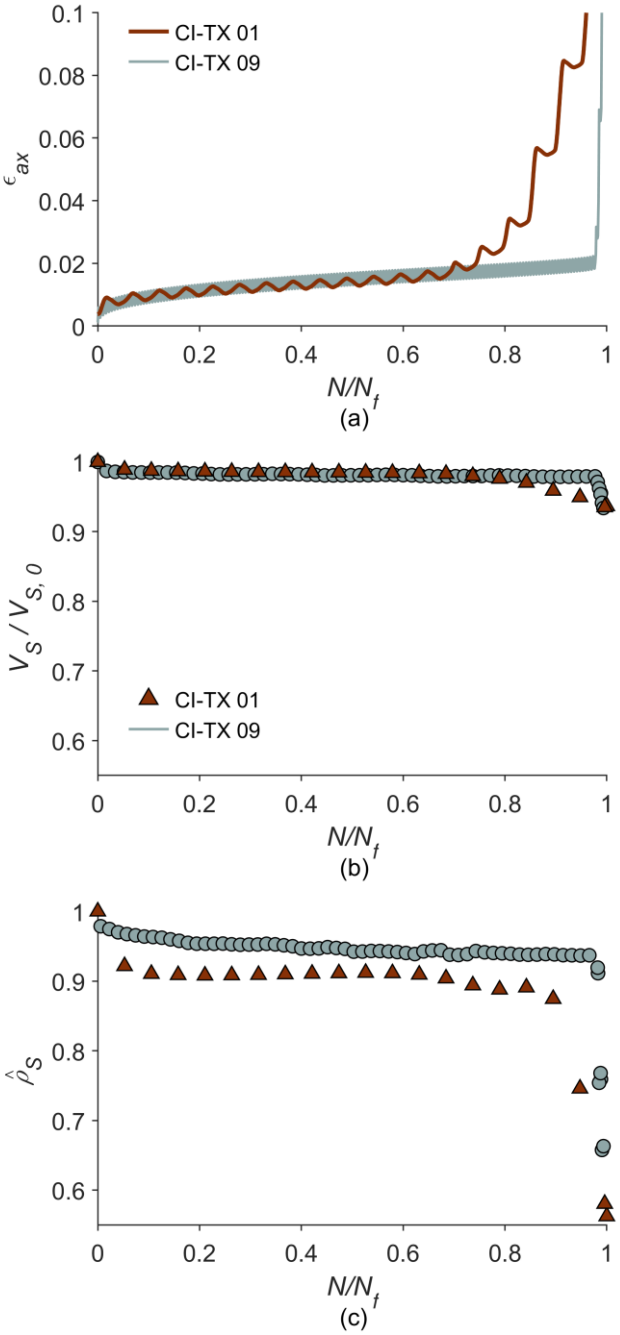

Figure 8: Evolution of the intact material state upon cyclic loading for tests CI-TX 01 and CI-TX 09: (a) effective mean stress p'; (b) normalized S-wave velocity $V_S / V_{S,0}$; and (c) normalized S-wave cross-correlation coefficient $\hat{\rho}_S$

3.3 Fatigue Loading

The results of two cyclic tests on intact specimens (see Table 1) are plotted in Figure 8 as a function of cycle number normalized to fatigue life N / N_f. The stress-controlled cyclic loading induces inelastic axial strain accumulation, leading to progressive destructuration and ultimately brittle failure (Figure 8a). In the first cycle, a sudden (although limited in amplitude) drop in $V_S / V_{S,0}$ is observed, likely due to initial pore pressure build-up (Ciancimino et al., 2026), while subsequently it stabilizes (Figure 8b). As failure approaches, $V_S / V_{S,0}$

217 further decreases, following the trends observed for ε_{ax}. Consistently with the monotonic tests, the decrease
218 is quite limited, with $V_S / V_{S,0}$ reaching a minimum of 0.94.

219 Similar trends are shown by the $\hat{\rho}_S$ evolution, which closely follows the brittle material response during
220 fatigue loading (Figure 8c). However, its decrease is more pronounced, dropping to 0.6 as the specimens
221 approach failure, indicating stronger sensitivity of $\hat{\rho}_S$ to material degradation with respect to $V_S / V_{S,0}$.

222 # 4 Discussion and conclusions

223 The in-situ state of caprocks must be properly monitored during seasonal gas storage operations, as cyclic
224 loadings can potentially compromise the formation integrity. The S-wave velocity is an attractive monitoring
225 parameter, as it is strongly influenced by the material structure and therefore affected by degradation. This is
226 partially confirmed by the experimental results presented here, as V_S decreases during mechanical loading.
227 However, the amplitude of the reduction is quite small. For brittle materials, failure is associated with the
228 formation of well-defined shear bands within which the degradation process occurs. In laboratory tests, V_S is
229 calculated as an average with respect to the specimen height, considering also those parts that are not affected
230 by destructuration. Therefore, the detected V_S changes are barely visible, although in principle large variations
231 are to be expected in correspondence of the shear band. The same phenomenon is expected to occur in-situ,
232 with the possible formation of shear banding patterns induced by fatigue loading. These would be difficult to
233 detect by averaged measurements, given the additional uncertainties of in-situ measurements.

234 An alternative lies in the analysis of the changes in amplitude and shape of acquired signals that occur as
235 the material approaches failure. Shear banding affects the propagation path of transmitted waves, resulting in
236 reflected and refracted waves that alter the received signals. These changes could be tracked using the S-wave
237 cross-correlation coefficient $\hat{\rho}_S$ computed between two successive acquisitions. The evolution of $\hat{\rho}_S$ is
238 strongly influenced by the degradation process, with a decrease of about 40% under both monotonic and cyclic
239 conditions when approaching failure. In addition, $\hat{\rho}_S$ also appears to be a sensitive index of different
240 mechanical behaviours. The same material can exhibit either a brittle or a ductile response depending on the
241 confining pressure and the initial state (i.e. intact or reconstituted). Consistently, $\hat{\rho}_S$ will evolve differently,
242 showing either a gradual or abrupt drop as the peak shear strength is approached.

243 The consistency of the results obtained under different loading and initial state conditions, together with
244 the magnitude of the observed variations, suggest that $\hat{\rho}_S$ could be a viable parameter for monitoring the

245 evolution of the material state on site. However, to confidently attribute the measured changes to the evolution
246 of the material state, repeatable and well-controlled source-receiver geometries must be adopted, such as those
247 of near-well or permanently installed monitoring systems.

Data availability

Data will be made available upon reasonable request.

Acknowledgments

Funding was provided by ENI SpA within the project “Hynergy”. The authors gratefully thank Eni SpA for the authorization to publish this work.

References

Aminu, M. D., Nabavi, S. A., Rochelle, C. A., & Manovic, V. (2017). A review of developments in carbon dioxide storage. *Applied Energy, 208*, 1389-1419. doi:10.1016/j.apenergy.2017.09.015

Burland, J. B., Rampello, S., Georgiannou, V. N., & Calabresi, G. (1996). A laboratory study of the strength of four stiff clays. *Geotechnique, 46*(3), 491-514. doi:10.1680/geot.1996.46.3.491

Barla, G., Barla, M., & Debernardi, D. (2010). New triaxial apparatus for rocks. *Rock Mechanics and Rock Engineering, 43*(2), 225-230. doi:10.1007/s00603-009-0076-7

Benetatos, C., Rocca, V., Verga, F., Adinolfi, L. & Marzano, F. (2023). Deformation behavior of a regional shale formation from integrated laboratory and well data analysis: insights for underground fluid storage in Northern Italy. *Geoenergy Sci. Engng,* 229, 212109, 10.1016/j.geoen. 2023.212109.

Ciancimino, A., Cosentini, R., Foti, S., Messori, A., Ullah, H., Volonté, G., & Musso, G. (2024). A preliminary investigation on the mechanical behaviour of a stiff Italian clay in the context of hydrogen storage. *Geomechanics for Energy and the Environment, 38*. doi:10.1016/j.gete.2024.100562

Ciancimino, A., Cosentini, R., Foti, S., Volonté, G., & Musso, G. (2026). Experimental investigation on the monotonic and cyclic behaviour of a structured clay at high confinement. *Geotechnique,* 1-13. doi.org/10.1680/jgeot.25.00524

Clayton, C. R. I. (2011). Stiffness at small strain: Research and practice. *Geotechnique, 61*(1), 5-37. doi:10.1680/geot.2011.61.1.5

Dutta, T. T., Otsubo, M., Kuwano, R., & O'Sullivan, C. (2020). Evolution of shear wave velocity during triaxial compression. *Soils and Foundations, 60*(6), 1357-1370. doi:10.1016/j.sandf.2020.07.008

Falcon-Suarez, I., North, L., Amalokwu, K., & Best, A. (2016). Integrated geophysical and hydromechanical assessment for CO2 storage: shallow low permeable reservoir sandstones. *Geophysical Prospecting, 64*(4), 828-847. doi:10.1111/1365-2478.12396

Ferreira, C., Rios, S., Cristelo, N. & Viana da Fonseca, A. (2021). Evolution of the optimum ultrasonic testing frequency of alkali-activated soil–ash. *Geotechnique Letters*, 11(3), 158-163. doi: 10.1680/jgele.21.00041

Heinemann, N., Alcalde, J., Miocic, J. M., Hangx, S. J. T., Kallmeyer, J., Ostertag-Henning, C., . . . Rudloff, A. (2021). Enabling large-scale hydrogen storage in porous media-the scientific challenges. *Energy and Environmental Science, 14*(2), 853-864. doi:10.1039/d0ee03536j

Jeanne, P., Zhang, Y., & Rutqvist, J. (2020). Influence of hysteretic stress path behavior on seal integrity during gas storage operation in a depleted reservoir. *Journal of Rock Mechanics and Geotechnical Engineering, 12*(4), 886-899. doi:10.1016/j.jrmge.2020.06.002

Mavko, G., Mukerji, T. & Dvorkin, J. (1998). The Rock Physics Handbook: Tools for Seismic Analysis in Porous Media. Cambridge University Press, 208-210.

Musso, G., Cosentini, R.M., Foti, S., Comina, C., Capasso, G. (2015). Assessment of the structural representativeness of sample data sets for the mechanical characterization of deep formations. *Geophysics*, 80 (5). doi:10.1190/geo2014-0351.1

Montoya, B. M., & De Jong, J. T. (2015). Stress-strain behavior of sands cemented by microbially induced calcite precipitation. *Journal of Geotechnical and Geoenvironmental Engineering, 141*(6). doi:10.1061/(ASCE)GT.1943-5606.0001302

Santamarina, J. C., Klein, K. A. & Fam, M. A. (2001), Soils and Waves: Particulate materials behavior, characterization and process monitoring, Wiley, ISBN: 0-47I-49058-X.

Shibuya, S. (2000). Assessing structure of aged natural sedimentary clays. *Soils and Foundations, 40*(3), 1-16. doi:10.3208/sandf.40.3_1

296 Stanchits, S., Vinciguerra, S., & Dresen, G. (2006). *Ultrasonic velocities, acoustic emission characteristics and crack*
297 *damage of basalt and granite.* Paper presented at the Pure and Applied Geophysics.

298 Xiao, J. Q., Ding, D. X., Jiang, F. L., & Xu, G. (2010). Fatigue damage variable and evolution of rock subjected to cyclic
299 loading. *International Journal of Rock Mechanics and Mining Sciences, 47*(3), 461-468.
300 doi:10.1016/j.ijrmms.2009.11.003

301 Zhou, Y. G., & Chen, Y. M. (2005). Influence of seismic cyclic loading history on small strain shear modulus of saturated
302 sands. *Soil Dynamics and Earthquake Engineering, 25*(5), 341-353. doi:10.1016/j.soildyn.2005.03.001